Zhao *et al. Hepatoma Res.* 2025;10:12
DOI: 10.20517/2394-5079.2024.143

Hepatoma Research

Original Article

Open Access

Predicting microvascular invasion plus cytokeratin 19 expression positivity in hepatocellular carcinoma based on EOB-MRI using multitask deep learning

Yuanyuan Zhao[1,2,#], Xiang Huang[3,#], Meili Sun[4,#], Jia Chen[5], Jian Zhang[6,7], Shi-ting Feng[8], Jianpeng Li[3], Kangyang Cao[9], Jifei Wang[8], Bingsheng Huang[2], Yujian Zou[3]

[1]Nuclear Medicine Department, The Seventh Affiliated Hospital, Sun Yat-sen University, Shenzhen 518107, Guangdong, China.
[2]Medical AI Lab, School of Biomedical Engineering, Medical School, Shenzhen University, Shenzhen 518055, Guangdong, China.
[3]Department of Radiology, The Tenth Affiliated Hospital of Southern Medical University (Dongguan People's Hospital), Dongguan 523059, Guangdong, China.
[4]Department of Radiology, Sun Yat-sen University Cancer Center, Guangzhou 510060, Guangdong, China.
[5]Active Medical Devices Testing Department, Shenzhen institute for drug control, Shenzhen 518034, Guangdong, China.
[6]Shenzhen-Hong Kong Institute of Brain Science-Shenzhen Fundamental Research Institutions, Shenzhen 518055, Guangdong, China.
[7]Medical School, Shenzhen University, Shenzhen 518060, Guangdong, China.
[8]Department of Radiology, Sun Yat-sen University Affiliated First Hospital, Guangzhou 510080, Guangdong, China.
[9]Faculty of Applied Sciences, Macao Polytechnic University, Macao 999078, China.
[#]These authors contributed equally to this work.

Correspondence to: Prof. Yujian Zou, Department of Radiology, The Tenth Affiliated Hospital of Southern Medical University (Dongguan People's Hospital), No.78 Wan Dao Road, Xingu Yong, Wanjiang Street, Dongguan 523059, Guangdong, China. E-mail: zouyujian@sohu.com; Prof. Bingsheng Huang, Medical AI Lab, School of Biomedical Engineering, Medical School, Shenzhen University, No.1066 Xueyuan Avenue, Taoyuan Street, Nanshan District, Shenzhen 518055, Guangdong, China. E-mail: huangbs@gmail.com; Prof. Jifei Wang, Department of Radiology, Sun Yat-sen University Affiliated First Hospital, No.58 Zhong Shan Er Lu Road, Yuexiu District, Guangzhou 510080, Guangdong, China. E-mail: wjif@mail.sysu.edu.cn

How to cite this article: Zhao Y, Huang X, Sun M, Chen J, Zhang J, Feng St, Li J, Cao K, Wang J, Huang B, Zou Y. Predicting microvascular invasion plus cytokeratin 19 expression positivity in hepatocellular carcinoma based on EOB-MRI using multitask deep learning. *Hepatoma Res.* 2025;10:12. https://dx.doi.org/10.20517/2394-5079.2024.143

Received: 12 Dec 2024 **First Decision:** 10 Mar 2025 **Revised:** 31 Mar 2025 **Accepted:** 17 Apr 2025 **Published:** 27 Apr 2025

Academic Editors: Matthias Ocker, Francesco De Cobelli **Copy Editor:** Shu-Yuan Duan **Production Editor:** Shu-Yuan Duan

Abstract

Aim: To construct and validate a multitask deep learning (DL) model based on gadolinium ethoxybenzyl diethylenetriamine pentaacetic acid (Gd-EOB-DTPA) contrast-enhanced magnetic resonance imaging (MRI) for predicting microvascular invasion (MVI) plus cytokeratin 19 (CK19) positivity in patients with hepatocellular carcinoma (HCC).

Methods: A total of 145 pathologically confirmed HCC patients undergoing preoperative enhanced MRI were assessed between January 2012 and January 2023. A predictive model, whose skeleton structure was an expert shared network based on spatial transformations and relational reasoning, was established based on hepatobiliary phase (HBP) images using a training set (*n* = 66, Center 1) and validated using an external (*n* = 79, Centers 2 and 3) test set. A receiver operating characteristic (ROC) curve was used to evaluate MVI CK19 positivity.

Results: The area under the ROC curve (AUC) of the new model, named Expert Sharing Network, for the prediction of the CK19 and MVI expression was 0.87 and 0.88 in the training set and 0.80 and 0.85 in the validation set, respectively, which was superior to the ResNeSt50-based model, EfficientNet-b0-based model, and ResNet50-based model. The AUC of the DL model for the prediction of the MVI was 0.88 in the training set and 0.85 in the validation set, which was superior to the other three models.

Conclusion: This new model can accurately predict CK19 expression and MVI in patients with HCC.

Keywords: Hepatocellular carcinoma, cytokeratin 19, microvascular invasion, deep learning, multitask learning

INTRODUCTION

Hepatocellular carcinoma (HCC) accounts for approximately 90% of all liver cancer cases[1]. Despite advances in treatment options, its incidence is growing worldwide, and these trends are expected to remain through 2030[2]. Long-term outcomes are affected by a high recurrence rate (up to 70% of cases 5 years after treatment)[2]. Thus, searching for new methods to predict early postoperative recurrence is paramount.

The treatment plan and prognosis of HCC are influenced by factors such as tissue differentiation[3], tumor number[4], satellite nodules[5], microvascular invasion (MVI)[6], and related genetic phenotypes[7]. For example, the positive expression of CK19, a cytoskeleton protein in liver precursor and bile duct cells, indicates a high risk of invasive HCC[8,9]. Moreover, MVI, characterized by cancer cell clusters in small vein branches, is linked to more aggressive tumor biology[6,10]. MVI has been recognized as an independent predictor of early recurrence and poor prognosis after liver resection or liver transplantation[11]. According to available clinical data, liver transplantation or radiofrequency ablation is not recommended for HCC patients with MVI; more specifically, anatomical or partial liver resections with wide resection margins should be used to improve the prognosis[12]. A correlation between CK19 expression and MVI has also been reported. In their study, Qin *et al.*[13] compared CK19 and MVI in 352 HCC patients and found that the CK19 + /MVI + group had the lowest disease-free survival and overall survival rates compared to CK19+ and MVI+ groups, suggesting that combining CK19 and MVI may predict postresection prognosis better than using either factor on its own. Research indicates that MVI is an important independent risk factor for postoperative recurrence and poor prognosis in HCC. The incidence of MVI is significantly higher in CK19-positive tumors compared to CK19-negative tumors[14,15]. CK19 is a marker of cholangiocyte differentiation, but it can be abnormally expressed in HCC, indicating that the tumor has a higher invasiveness[14]. Studies have shown that CK19-positive HCC patients are more likely to experience MVI, which may be related to tumor stem cell characteristics, activation of epithelial-mesenchymal transition (EMT), and upregulation of pro-angiogenic factors such as vascular endothelial growth factor[15-18]. MVI is an important independent risk factor for postoperative recurrence and poor prognosis in HCC. The incidence of MVI in CK19-positive tumors is significantly higher than in CK19-negative tumors[14,15]. Patients with CK19-positive tumors combined with MVI have a significantly increased early postoperative recurrence rate, poorer response to targeted therapy, and shorter survival[9,16,19,20]. Additionally, evaluating CK19 and MVI can provide a more comprehensive reflection of tumor heterogeneity and aggressiveness, assisting clinicians in: screening high-risk patients, optimizing surgical and adjuvant treatment strategies;

avoiding undertreatment or overtreatment to enhance survival benefits; and establishing dynamic prognostic models to guide individualized follow-up. Therefore, preoperative prediction of MVI and CK19 expression in HCC is considered crucial for determining treatment and improving prognosis. Yet, the diagnosis of CK19 and MVI is mainly based on postoperative histologic examination, usually known only several days after surgery, limiting its use to direct postoperative care. Additionally, during this process, only specific tissue areas are collected, failing to fully represent the whole lesion mass.

Magnetic resonance imaging (MRI) is the optimal method for diagnosing, staging, and evaluating treatment efficacy in HCC[21]. Gd-EOB -DTPA-enhanced MRI can reflect the biological behavior of HCC and its tumor microenvironment[22]. The HBP, post-contrast injection time range after administration of a hepatobiliary agent, is an important stage of Gd-EOB-DTPA-enhanced MRI. Compared to traditional MRI, Gd-EOB-DTPA-enhanced MRI has a higher detection rate of MVI positivity in the HBP, enabling earlier detection of MVI and aiding in developing more effective treatment strategies[23-25], providing clinicians with useful information regarding invasion and prognosis of HCC. Furthermore, studies have shown that imaging features from Gd-EOB-DTPA-enhanced MRI can help predict CK19 expression[26] and MVI[27] before surgery. However, despite offering important macroscopic imaging characteristics, the limited greyscale range of visual images restricts its potential application in reflecting detailed microscopic features.

With the rapid development of computer technology, machine learning methods, including radiomics and DL programs, have been widely applied in medical imaging analysis. Wang *et al.*[28] constructed a radiomics prediction model based on a fusion radiomics signature derived from arterial and hepatobiliary phase images of Gd-EOB-DTPA-enhanced MR for evaluating the CK19 status of HCC. Moreover, Feng *et al.*[29] developed a radiomics prediction model for preoperative MVI in HCC based on Gd-EOB-DTPA-enhanced MRI, achieving significant accuracy in training and validation sets. However, radiomics still has certain limitations, including the subjective design of extracted features, strong data dependency, poor feature generalization, and the requirement for doctors to manually delineate tumors layer by layer, which is time-consuming and labor-intensive[30].

DL methods offer a direct feature extraction from MRI, eliminating the need for manual design. Only tumor framework outlining is required, enhancing model generalization and repeatability. Chen *et al.*[31] used a convolutional neural network (CNN) to establish a DL model for preoperative prediction of CK19 expression in Gd-EOB-DTPA-enhanced MRI, achieving AUCs of 0.820 and 0.781 in the training and external validation sets, respectively. Additionally, Wang *et al.*[32] compared 2D, 2D-expansion, and 3D DL models for HCC MVI prediction based on Gd-EOB-DTPA-enhanced MRI, finding comparable performance between 2D-expansion and 3D DL models, with AUC values of 0.70 and 0.72, respectively.

However, the above studies involved single-task DL models. Single-task learning trains models separately for each task, resulting in the need to learn features from scratch for each model. For related tasks (e.g., predicting CK19 and MVI), certain underlying features (e.g., vascular pattern or heterogeneity of tumors) may be shared. Single-task learning cannot utilize these shared features, leading to redundancy in feature extraction and waste of computational resources[33-35]. Moreover, single-task learning requires a large amount of annotated data to be prepared separately for each task, while multitask learning can improve data efficiency by sharing data and feature representations. For example, the prediction tasks of CK19 and MVI can share some of the labeled data (e.g., features of the tumor region), thus reducing the need for separate labeled data for each task[36]. Thus, single-task learning suffers from limitations such as feature redundancy, ignoring inter-task correlation, data inefficiency, limited generalization ability, and wasted computational resources when dealing with multiple related tasks.

In contrast, multitask learning can effectively overcome these limitations by sharing feature representations and jointly training multiple tasks, thus improving model performance and efficiency[34]. It learns shared information among tasks and uncovers crucial information for individual tasks, enhancing task accuracy and generalization[34]. Fan *et al.*[37] demonstrated the effectiveness of multitask learning in predicting breast cancer tissue grading and Ki-67 expression levels based on dynamic contrast-enhanced magnetic resonance imaging (DCE-MRI) and diffusion-weighted imaging (DWI) simultaneously, outperforming single-task models with AUC values of 0.811 and 0.816, respectively. Thus, it is believed that multitask learning methods can assist a single task in achieving better performance by training and learning from multiple relevant tasks.

In this study, we constructed a multitask DL model based on Gd-EOB-DTPA-enhanced HCC MRI, validated on an external test set using pathological histology. We hypothesized that the multitask DL model can simultaneously predict the expression of CK19 and the presence of MVI and that its predictive performance exceeds that of single-task DL models.

METHODS

Patients

This study adheres to the Declaration of Helsinki and has obtained approval from the Ethics Committees of Sun Yat-sen University Affiliated First Hospital (Center 1), Sun Yat-sen University Cancer Center (Center 2), Southern Medical University Tenth Affiliated Hospital (Dongguan People's Hospital) (Center 3). In accordance with the approvals, the requirement for informed consent was waived. The reasons were as follows: (1) due to the retrospective nature of this study, it was unrealistic or impossible to obtain informed consent from all patients; (2) the study did not exceed the minimum risk after review by the ethics committees; (3) all patient data accessed complied with relevant data protection and privacy regulations; (4) the rights and interests of all patients have not been invaded.

This study retrospectively collected Gd-EOB-DTPA-enhanced MRI data from patients admitted to the three centers between January 2012 and January 2023. Data regarding inclusion and exclusion criteria can be found in the Supplementary Materials. The study flow chart is shown in Figure 1.

MRI

MRI scan in Center 1, Center 2, and Center 3 utilized a Magnetom Trio A Tim 3.0T system (Siemens Healthcare Sector, Erlangen, Germany), GE 3.0T (750W, Pioneer; GE Healthcare, Milwaukee, WI) MR scanning system, and Magnetom Skyra 3.0 T system (Siemens Healthcare Sector, Erlangen, Germany), respectively. The scanning covered the top to the lower edge of the liver with an 18-channel or 8-channel phased-array coil as the receiver coil. Gd-EOB-DTPA-enhanced MRI was obtained including the unenhanced phase, enhanced arterial phase (20-40 s), portal phase (50-70 s), equilibrium phase (100-120 s), transitional period (3-5 min), and 20- min HBP images. Gd-EOB-DTPA (Primegen; Bayer Schering Pharma, Berlin, Germany) was injected into the cubital vein at a flow rate of 1 mL/s and a dose of 0.025 mmol/kg, followed by 20 mL of normal saline for flushing. A more detailed description of the MRI methods and specific sequences and parameters of MRI scans are shown in Supplementary Table 1.

The resident radiologist first contoured the ground truth of tumor lesions on the HBP in HCC patients (with 3 years of experience in the field), and this was then reviewed by a more experienced radiologist (with 15 years of experience in the field); both radiologists were blinded to clinical and pathological data. If the opinions of the contour between the two radiologists were different, a discussion would be held until a consensus was reached. The radiologist labeled three layers, including the first, the largest, and last layer of

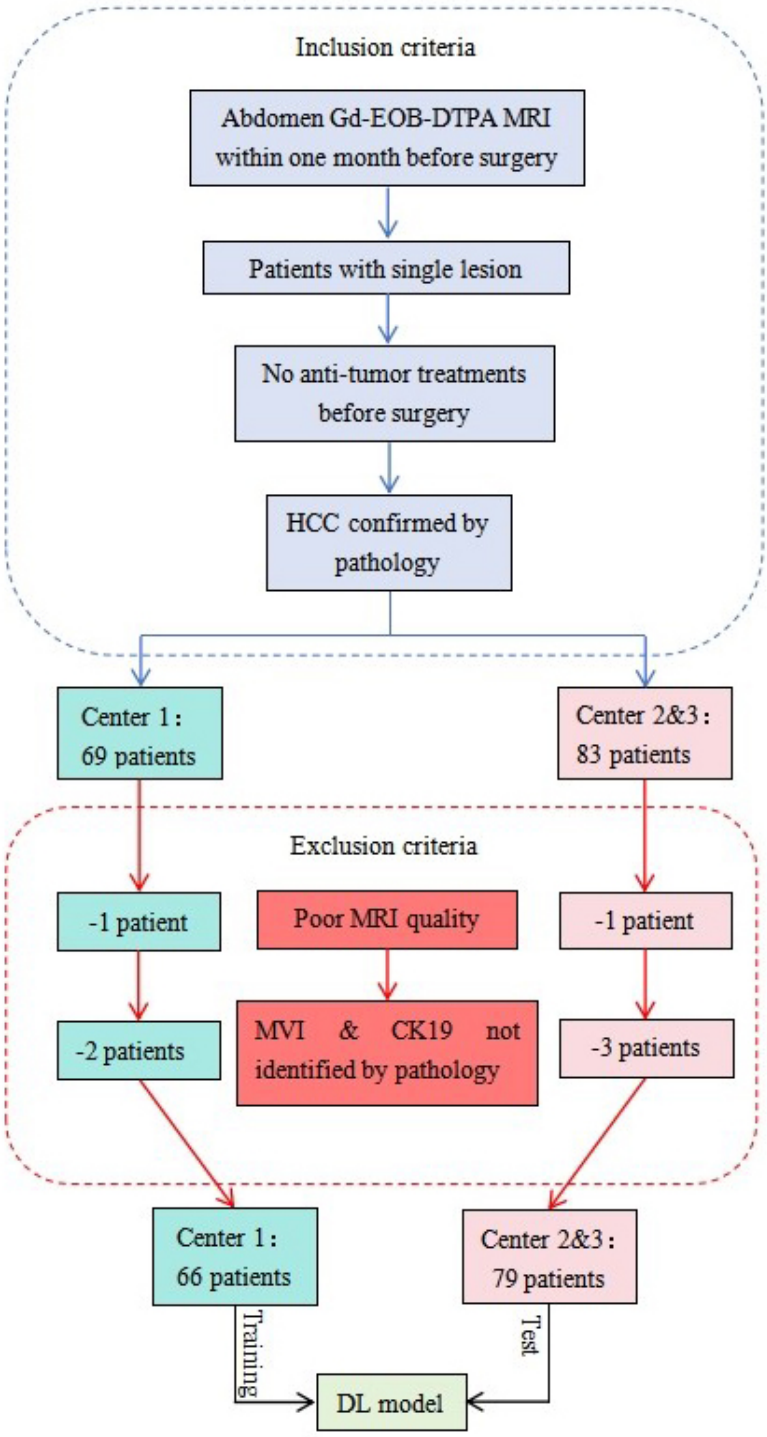

Figure 1. Study flowchart.

tumor appearance on cross-section MRI based on Insight Toolkit (ITK)- snap software. MVI was defined as as the invasion of tumor cells within a vascular space lined by endothelium that is visible only on microscopy[38-40]. Data were collected in strict accordance with the diagnostic guideline[40]. To avoid possible missing data, the volume of interest (VOI) in MR images covered the whole tumor and peritumor region[41].

The marked quadrangles all contained tumor areas, as seen in Figure 2.

Clinicopathological analyses

HCC specimens were pathologically sampled following standardized guidelines[39]. Diagnostic criteria were based on World Health Organization morphological standards[42,43]. Two pathologists (with over 10 years of HCC pathology experience) who were blinded to clinical and imaging information independently reviewed all specimens. MVI, identified as tumor emboli in endothelial-lined vascular spaces on microscopy[42], and CK19 expression, assessed semiquantitatively through immunochemical staining, were determined. Tumors were classified as negative (< 5% of tumor cells) or positive (≥ 5% of tumor cells) for CK19.

Training and validation of deep learning models

Our framework, depicted in Figure 3, adopts ResNeSt[44] as the backbone of the DL model. Compared with commonly used classification networks, ResNet[45] introduces a residual module with skip connections to alleviate the vanishing gradient problem, while EfficientNet[46] achieves balanced scaling by simultaneously adjusting the network depth, width, and input image resolution. Building on ResNet, ResNeSt incorporates a split-attention module to enhance task accuracy while reducing the amount of computation. For a more detailed network structure, see the deep learning classification algorithms section of Supplementary Materials.

To address the negative transfer between tasks and the phenomenon where one task performance improves while another performance declines in most multitask learning algorithms, we designed a network structure named "Expert Sharing Network". Its basic structure with the currently used multitask learning algorithms is shown in Figure 3.

As shown in Figure 3A, the CK19 expression prediction and MVI prediction tasks in the Hard Parameter Sharing Network model share a feature extraction module, which may lead to negative migration in the network due to weak correlation or conflict of tasks. It is also possible that the feature-sharing module of the network model may be dominated by one task so that it mainly fits that task, resulting in an increase in the performance of one task and a decrease in the performance of the other[47]. The Cross-Stitch Network model of Figure 3B automatically adjusts the degree of sharing between tasks by changing the task weight parameter in the module, which solves the negative network migration phenomenon to a certain extent, but there still exists the situation that the performance of one task rises while the performance of another task falls[48]. The core idea of the Expert Sharing Network [Figure 3C] is to clearly separate the common shared task parameters from the individual task-specific parameters, thus avoiding the complex parameter sharing that brings instability to the network model. The feature extraction part of the network is split into three sub-networks: sub-network 1, dedicated solely to CK19 expression prediction; sub-network 2, focused exclusively on MVI prediction; and the expert sharing sub-network responsible for learning shared features. This will help to avoid situations where complex parameter sharing causes the network to be biased toward fitting a particular task, causing the network model to experience negative migration and a rise in performance for one task and a drop in performance for the other. The Expert Sharing Network is detailed in the multitask learning framework section of Supplementary Materials.

Additionally, in order to further assess the potential relationships between tasks and improve the predictive performance of the model, the Spatial Transformation Module (STN)[49] and Relation Reasoning Module (RN)[50] were introduced into the network. The detailed structure of the above modules can be found in the network structure of improvement section of Supplementary Materials. Our framework is shown in Figure 4.

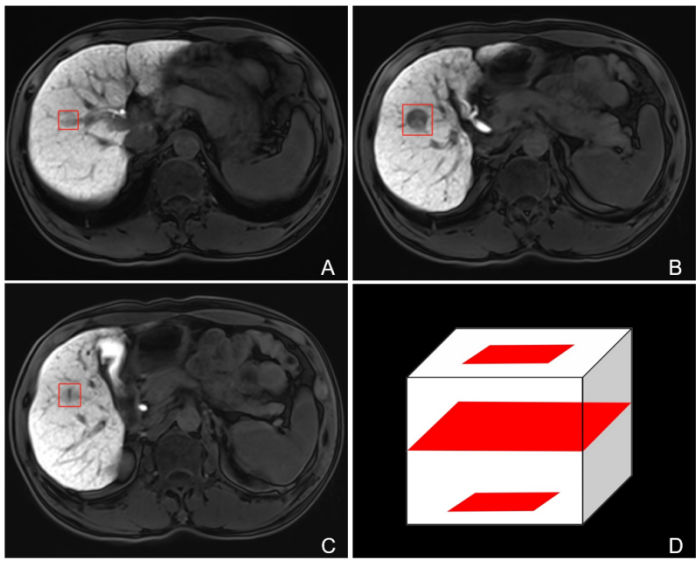

Figure 2. Lesion contouring for deep learning analysis. The first layer (A), the largest layer (B), and the last layer (C) of the tumor were outlined by a radiologist to build a cube area of interest, including the whole tumor lesion (D).

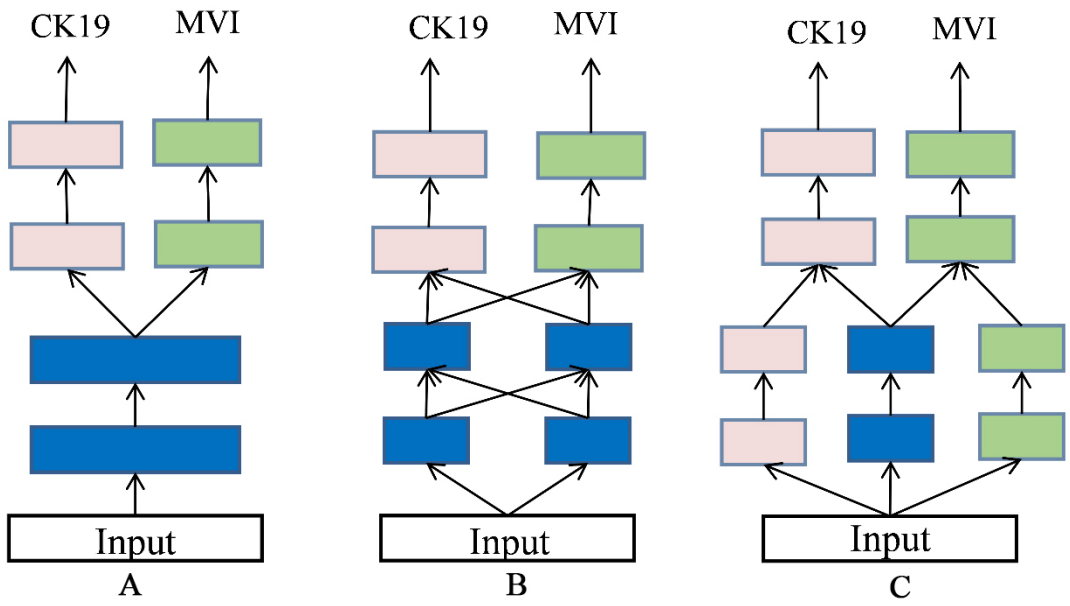

Figure 3. Basic structures of multitask learning networks. (A) The hard parameter sharing network; (B) The Cross-Stitch Network; (C) The expert-sharing network.

In this study, the dataset of Center 1 was used to establish the network model. To avoid model overfitting, we used 10-fold cross-validation to train the model, resulting in 10 models. The best-performing model from cross-validation was selected, and the datasets from Center 2 and Center 3 served as external independent test sets to validate the robustness of the algorithm.

The network model was trained and tested using Nvidia GTX 1080TI graphics cards with 11GB of memory. The network model was built using the PyTorch DL framework. The network autonomously learns linear

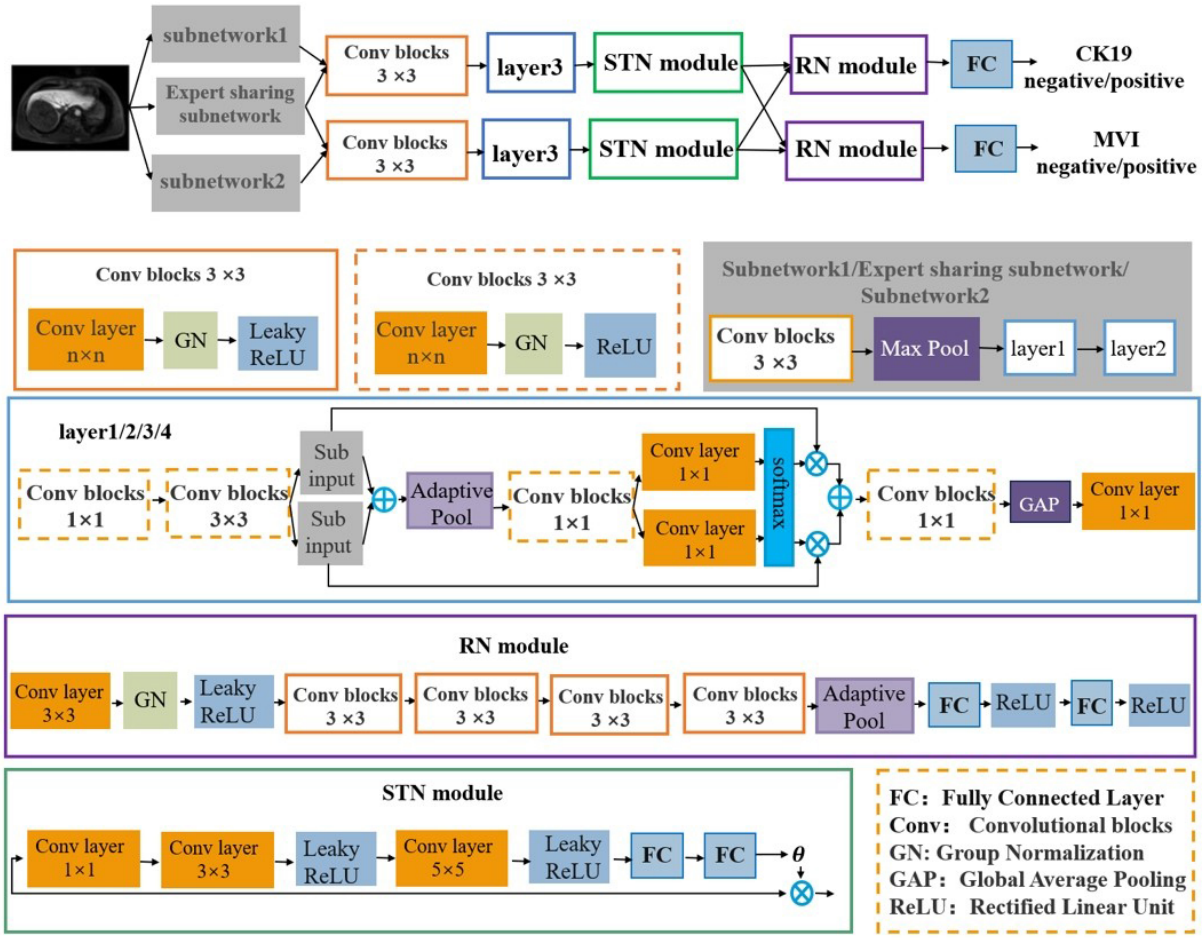

Figure 4. Expert Sharing Network structure based on spatial transformation and relation reasoning.

combinations of weights based on tasks in order to selectively fuse representations from different tasks. Focal Loss was chosen as the training loss function, and the optimizer used was Adam, with a penalty factor of 0.05. The batch size during training was 16; the initial learning rate was 1s set; the total number of epochs was 300. The learning rate was decayed by a factor of 0.2 every 100 epochs.

Real-time data augmentation was applied to the training dataset to avoid overfitting due to insufficient training data. The augmentation methods included (1) image flipping; (2) random image cropping; (3) image scaling; (4) image translation; (5) image rotation; and (6) shear transformation.

To transform the continuous probability outputs of the deep learning model into binary predictions (MVI/CK19-positive *vs.* negative), the optimal cut-off value was determined by maximizing the Youden Index (J = sensitivity + specificity – 1). The ROC curve was generated using the validation set, and the threshold corresponding to the point closest to the top-left corner was selected as the cut-off. This approach balances sensitivity and specificity, ensuring minimal misclassification costs in clinical decision making.

We applied widely used DL classification algorithms, namely ResNet[45], EfficientNet[46], and ResNeSt[44,45], to the prediction tasks in this study. The performance of single-task methods on the HCC CK19 expression and HCC MVI prediction tasks was compared with the proposed multitask method, demonstrating the

superiority of the multitask approach. The specific network framework details can be found in the Supplementary Materials.

Statistical analysis

The performance of the network model was evaluated using accuracy, specificity, sensitivity, ROC curve, and AUC.

For the prediction of CK19 expression, we considered CK19-positive expressions as positive samples and CK19-negative expressions as negative samples; for MVI, samples classified as MVI-positive were considered positive samples, while non-MVI were considered negative samples.

RESULTS

Clinical and pathological data

Initially, 69 patients were enrolled from Center 1, 58 from Center 2, and 25 from Center 3. Subsequently, 3 patients from Center 1 and 4 from Centers 2 and 3 were excluded. Patients from Center 1 comprised the training set, while patients from Centers 2 and 3 comprised the test set. The Clinical Characteristics and Pathological Parameters for the Training and Test Sets are presented in Table 1. There were no differences in age, Child-Pugh class A score, number of CK19-positive patients, or number of MVI-positive patients between the training and test sets (all $P > 0.05$).

Prediction of CK19 expression in patients with HCC

The performance comparison of our proposed method with three single-task frameworks on HCC CK19 expression prediction is shown in Table 2. The MR images, together with the corresponding CK19 expression and MVI status, are illustrated in Figure 5. The ROC curves of different classification models for internal cross-validation and external independent testing on CK19 expression prediction are illustrated in Figure 6. The final cut-off value was determined to be 0.48. Precision-recall curves are shown in Supplementary Figure 1. When assessing patients in Center 1, our model (AUC = 0.87) proved to be superior to ResNeSt50-based model (AUC = 0.71), EfficientNet-b0-based model (AUC = 0.70), and ResNet50-based model (AUC = 0.67). Similar data were observed in Centers 2 and 3 (AUC values of 0.80, 0.70, 0.67, and 0.65 for the four models, respectively).

Prediction of MVI in HCC

The performance comparison of our proposed method with three single-task frameworks on HCC MVI prediction is shown in Table 3 and Figure 7. Precision-recall curves are shown in Supplementary Figure 2. When assessing patients in Center 1, our model (AUC = 0.88) proved to be superior to ResNeSt50-based model (AUC = 0.83), EfficientNet-b0-based model (AUC = 0.79), and ResNet50-based model (AUC = 0.72). Similar data were observed in Centers 2 and 3 (AUC values of 0.85, 0.79, 0.78, and 0.71 for the four models, respectively).

DISCUSSION

This is the first study to propose a multitask DL model based on Gd-EOB-DTPA-enhanced MRI to predict CK19 expression and MVI simultaneously in HCC. The multitask DL model outperformed single-task DL models in predicting CK19 expression and MVI, demonstrating robustness. The proposed approach in this study contributes to providing effective references for the clinical preoperative assessment of CK19 and MVI status, assisting physicians in guiding individualized management for HCC patients.

Table 1. Baseline clinical characteristics and pathological parameters in the training and test sets

Variables	Total *n* = 145	Training set *n* = 66	Test set *n* = 79	*P* value
Age (yrs)	54.1 ± 13.0	54.2 ± 14.0	54.1 ± 12.3	0.09
Sex (female)	29 (20%)	7 (11%)	22 (28%)	0.01*
History of hepatitis B	123 (85%)	62 (94%)	6 2(78%)	< 0.01*
Child-Pugh class A	140 (97%)	65 (98%)	75 (95%)	0.25
AFP > 400 μg/L	3 6 (25%)	22 (33%)	14 (18%)	0.03*
CK19-positive expression	44 (30%)	20 (30%)	24 (30%)	0.99
MVI-positive tissue	51 (35%)	25 (38%)	26 (33%)	0.53

*$P < 0.05$. Values are represented as mean ± standard deviation or number (percentage). *P* values represent the result of a comparison of the training set with the test set. CK19: cytokeratin 19; MVI: microvascular invasion; AFP: alpha-fetoprotein.

Table 2. Performance comparison of different classification models for HCC CK19 expression prediction

Experiment	Model	Accuracy (%)	Sensitivity (%)	Specificity (%)	AUC (%)
Internal cross-validation (Center 1)	ResNet50	64	85	54	67
	EfficientNet-b0	79	50	91	70
	ResNeSt50	70	60	74	71
	Expert sharing network	83	75	87	**87**
Independent external test (Centers 2 and 3)	ResNet50	74	75	73	65
	EfficientNet-b0	58	75	53	67
	ResNeSt50	74	75	73	70
	Expert sharing network	84	75	87	**80**

AUC: area under the receiver operating characteristic (ROC) curve.

Table 3. Performance comparison of different classification models for HCC MVI prediction

Experiment	Model	Accuracy (%)	Sensitivity (%)	Specificity (%)	AUC (%)
Internal cross-validation (Center 1)	ResNet50	71	68	73	72
	EfficientNet-b0	74	68	78	79
	ResNeSt50	80	76	83	83
	Expert sharing network	85	80	88	**88**
Independent external test (Centers 2 and 3)	ResNet50	79	67	85	71
	EfficientNet-b0	89	67	100	78
	ResNeSt50	79	83	77	79
	Expert sharing network	89	67	100	**85**

AUC:area under the receiver operating characteristic (ROC) curve; HCC: hepatocellular carcinoma.

In this study, there were no statistically significant differences in the proportion of patients by Age, Child-Pugh class A, CK19, and MVI between the Training and Test sets, suggesting that the prevalence of CK19-positive and MVI-positive HCC remained relatively constant across both sets.

In this study, DL classification algorithms, namely ResNet[45], EfficientNet[46] and ResNeSt[44], were employed for prediction tasks. Among the three models, ResNet50 performed the best. This could be attributed to the decentralized attention module introduced in ResNeSt, which integrates concepts from both the ResNeXt network and SENet. Compared to ResNet and EfficientNet, ResNeSt can improve task accuracy without incurring additional computational costs[44]. Therefore, ResNeSt was selected as the backbone network.

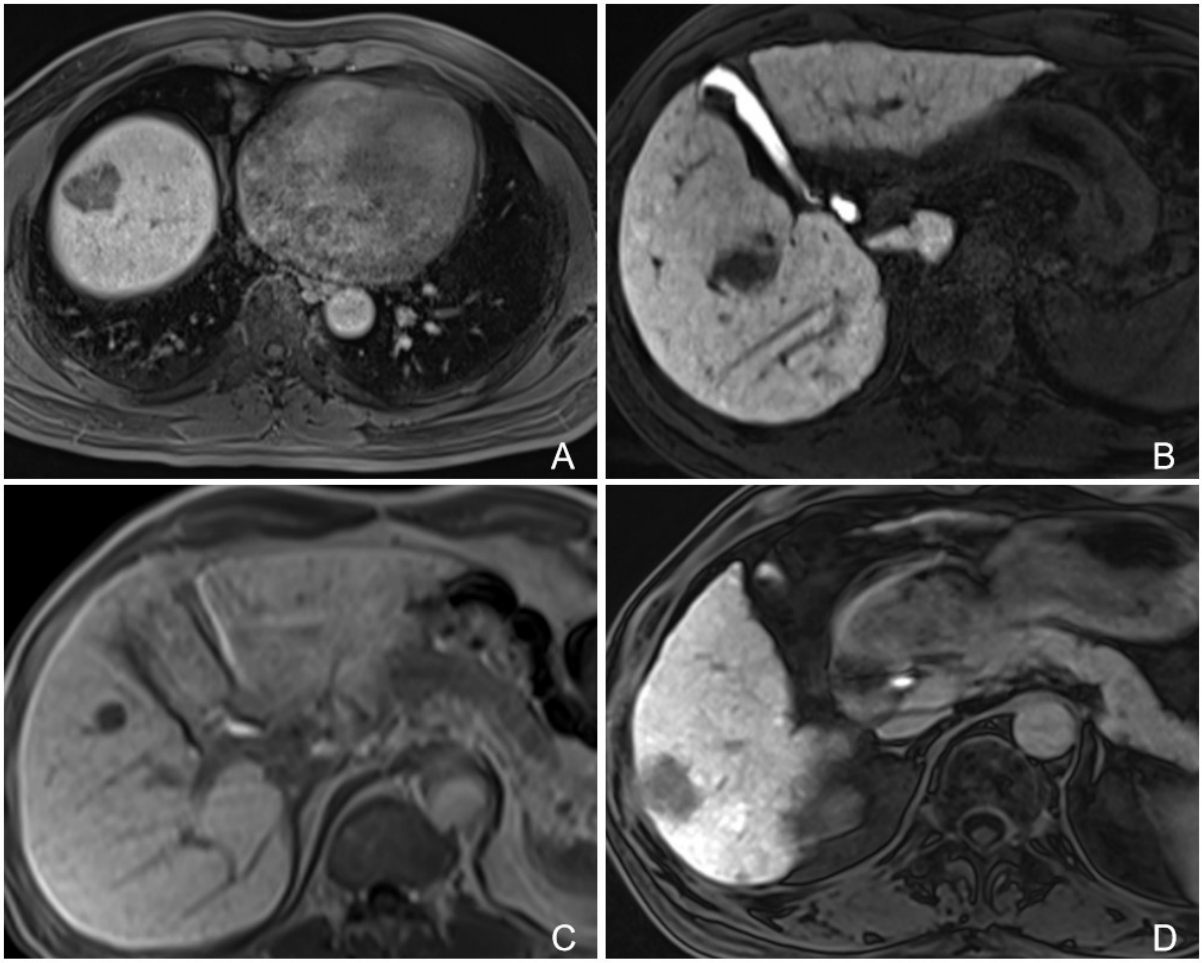

Figure 5. The MR images with the corresponding CK19 and MVI. (A)MVI- CK19+ (B) MVI+ CK19- (C) MVI- CK19+ (D) MVI+ CK19-. CK19: cytokeratin 19; MVI: microvascular invasion.

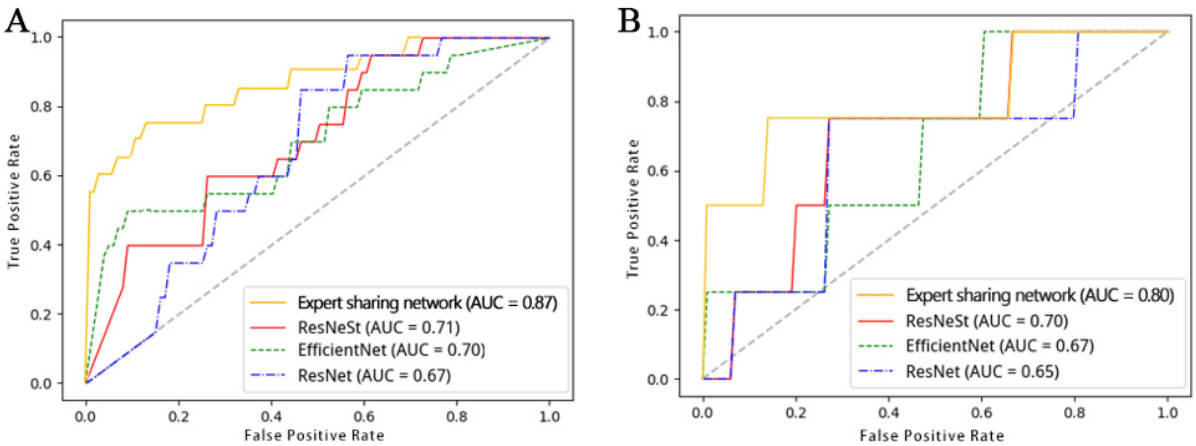

Figure 6. The ROC curves for predicting CK19 expression in patients with HCC. (A) Internal cross-validation; (B) external independent testing. AUC:area under the receiver operating characteristic curve; ROC: receiver operating characteristic; CK19: cytokeratin 19; HCC: hepatocellular carcinoma.

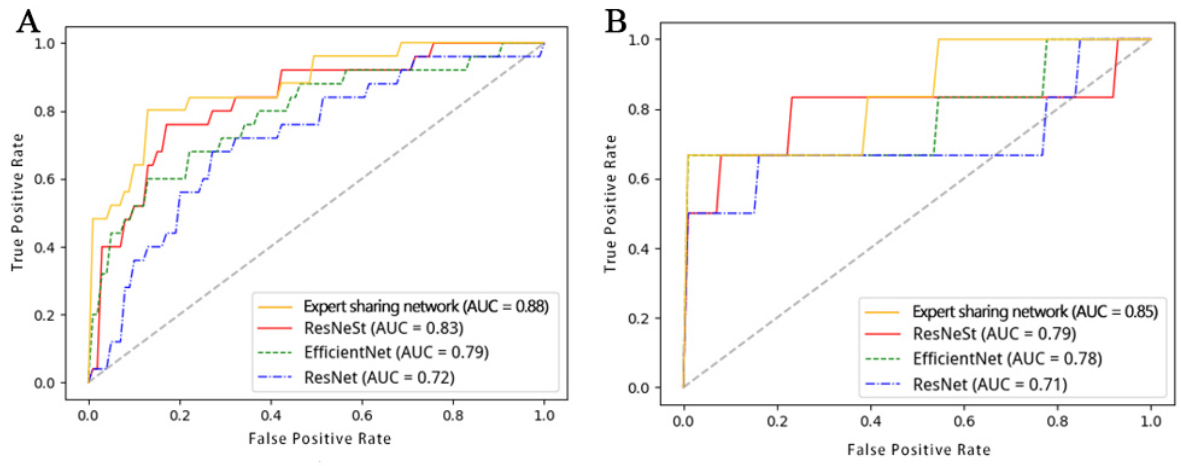

Figure 7. The ROC curves for predicting MVI in patients with HCC. (A) Internal cross-validation; (B) external independent testing. AUC:area under the receiver operating characteristic curve; ROC: receiver operating characteristic; MVI: microvascular invasion; HCC: hepatocellular carcinoma.

Few studies based on Gd-EOB-DTPA-enhanced MRI have assessed the predicted potential of CK19 expression in HCC. Chen *et al.*[31] developed and validated the performance of a DL radiomics model for CK19 identification in HCC based on Gd-EOB-DTPA-enhanced MRI, obtaining an internal validation set AUC of 0.82 and an external test set AUC of 0.781. In comparison, our single-task method yielded slightly lower performance. The main reason is that the previous method independently designed a deep semantic feature extraction module, which processed the enhanced MRI of HCC through a trained feature extraction model for semantic feature extraction. In contrast, our approach did not involve training a separate feature extraction model; instead, decentralized attention modules were used to extract features from ResNeSt. Moreover, Yang *et al.*[51] retrospectively included a multicenter, temporally independent cohort using a radiomics model based on enhanced MRI for CK19 expression prediction. The final AUCs for the training and two validation cohorts were 0.857, 0.726, and 0.790, respectively. Their performance was slightly superior to that of our single-task method, potentially because they created a composite model, whereas we constructed a simpler DL classification model.

Our multitask approach based on ResNeSt achieved excellent performance in predicting CK19 expression in HCC, with an AUC of 0.87 in the internal cross-validation set and 0.80 in the external independent test set [Table 2]. This result surpassed the performance of the ResNeSt network and was also slightly higher than the results reported in the literature mentioned above. The main reason is that the ResNeSt network and the methods proposed in the literature are based on a single-task framework for predicting CK19 expression. The information obtained by the network is only related to features associated with CK19 expression. In this study, we simultaneously performed multitask learning to predict CK19 expression and MVI in HCC. In addition to utilizing features related to CK19 expression, the network can also exploit the intrinsic relationship between CK19 expression and MVI, extracting shared information between the two tasks to improve the performance of CK19 expression prediction. Multitask learning can leverage the potential relationships between tasks to extract important information, thereby improving the accuracy and generalization capabilities of the tasks[52], as demonstrated in many studies. For example, Chu *et al.*[36] used multi-phase Gd-EOB-DTPA-enhanced MRI to establish a three-dimensional CNN (3D CNN) for single-task learning focused on predicting MVI and multitask learning simultaneously predicting MVI and vessels encapsulating tumor clusters (VETC). The results showed that the AUC of the 3D CNN for single-task

learning was 0.896, and multitask learning improved the performance of MVI prediction with an AUC value of 0.917. Similarly, we applied widely used DL classification algorithm networks to predict MVI in HCC [Table 3]. ResNeSt demonstrated the best performance (Internal AUC = 0.83, External AUC = 0.79). The superiority of the ResNeSt model in the framework contributes to these results. Some studies have also achieved accurate prediction of MVI in HCC based on Gd-EOB-DTPA-enhanced MRI.

Zhang *et al.*[53] developed a DL model based on multi-sequence MRI, achieving accurate preoperative prediction of MVI in HCC through enhanced MRI. The study utilized a 3D CNN to establish fusion models combining sequences. The final AUC of the fusion model in the training set was 0.81, and in the validation set, it was 0.72. The performance of this model was slightly inferior to that of the ResNeSt network in predicting MVI, possibly because ResNeSt uses average pooling layers instead of convolutional ones, reducing spatial information loss[50]. Additionally, Sun *et al.*[54] developed a DL model based on preoperative dynamic contrast-enhanced magnetic resonance imaging (DCE-MRI) to predict the MVI status in HCC. The resulting DL-based predictive model accurately predicted MVI risk, with an AUC of 0.824. The results were comparable to those obtained by the ResNeSt network. Although this study used a traditional CNN, it combined pathological predictive factors and employed a multi-input network, enabling the model to achieve performance comparable to the larger-parameter ResNeSt network.

Our multitask approach based on ResNeSt also demonstrated excellent performance in predicting MVI in HCC (Internal AUC = 0.88, External AUC = 0.85) [Table 3]. This result not only surpasses the performance of the ResNeSt network but is also slightly higher than the results reported in the literature mentioned above. When predicting MVI in HCC, our proposed multitask method utilized features related to MVI and exploited the intrinsic relationship between MVI and CK19 expression. This allows the network to extract shared information between the two tasks, enhancing the performance of MVI prediction.

However, there was a slight decrease in the results of the external test compared to the internal validation (e.g., CK19 AUC from 0.87 to 0.80, MVI AUC from 0.88 to 0.85), which may be attributed to the domain bias caused by differences in scanning equipment, parameters, or patient populations in different centers; in addition, CK19, as a biomarker, may be expressed heterogeneously in different centers, which affects the model to capture stable features. Meanwhile, training data from a single center may not be sufficient to cover all potential variant scenarios, resulting in insufficient model generalization ability. Multicenter joint training, biomarker-image correlation analysis, and model integration of clinical features may be able to solve the above problems, which will be explored in our future studies.

In summary, we have successfully proposed a predictive algorithm based on multitask learning and enhanced MRI, capable of accurately predicting CK19 expression and MVI in HCC. We designed an Expert Sharing Network that distinctly separates shared task parameters from specific task parameters, addressing negative transfer and the phenomenon where one task performance improves while another performance declines, which is commonly observed in multitask learning. Additionally, we adapted a Jaderberg[49] network, introducing a Spatial Transformation Module to learn useful affine transformations for task predictions autonomously. Applying these transformations can remove irrelevant noise, enhancing task classification. To further explore and leverage the relationship between CK19 expression and MVI, we improved a network based on Santoro[50], designing a Relation Reasoning Module. The purpose is to utilize the correlation between CK19 expression and MVI for more accurate predictions by the network model. Our results demonstrate that our proposed Expert Sharing Network, incorporating the Spatial Transformation Module and Relation Reasoning Module, achieved excellent performance in simultaneously predicting CK19 expression and MVI in HCC, which helps doctors assess prognosis and formulate

personalized treatment plans more accurately and facilitates close monitoring for early detection of tumor recurrence, leading to improved treatment outcomes and survival rates.

The present study has several limitations. First, we have not yet utilized other sequences from different phases of enhanced MRI. Previous literature has reported that data from different sequences and phases of enhanced MRI can provide rich feature information for predicting CK19 expression and MVI in HCC. Second, clinical information has not been integrated into the model, which could enhance predictive performance. Third, the skeleton network used in this study was not the latest classification network, and its performance may not be optimal. Further studies should explore and update classification networks to address these limitations. Additionally, the study will focus on utilizing clinical and pathological information from patients and exploring updated classification networks.

The multitask learning approach proposed in our study has good performance and robustness in predicting CK19 expression and MVI in HCC. This model could improve prognosis, develop more tailored treatment plans, improve treatment efficacy, and ultimately prolong patient survival, which may be a useful non-invasive method for preoperative prediction of CK19 expression and MVI in HCC.

DECLARATIONS

Authors' Contributions

Overall study design: Zou Y, Wang J, Zhang J
Supervised the data collection: Wang J, Sun M, Zou Y, Feng S, Huang B, Cao K, Chen J
Model building and training: Zhao Y
Data analysis: Zhao Y, Li J, Huang X
Manuscript drafting: Zhao Y, Li J
Manuscript editing: Zhao Y, Li J, Huang X, Huang B, Cao K, Zou Y, Zhang J, Wang J
Read, discussed, and approved the final version of the manuscript: Zhao Y, Huang X, Sun M, Chen J, Zhang J, Feng S, Li J, Cao K, Wang J, Huang B, Zou Y
All authors had full access to the data in the study and take responsibility for the integrity of the data and the accuracy of the data analysis, as well as the decision to submit for publication.

Availability of data and materials

The data that support the findings of this study are not openly available due to reasons of patient privacy and are available from the corresponding author upon reasonable request.

Financial support and sponsorship

This study received funding from Dongguan Science and Technology of Social Development Program(20221800906272), Natural Science Foundation of Guangdong Province (No.2022A1515011640), and National Natural Science Foundation of China(62371303).

Conflicts of interest

All authors declared that there are no conflicts of interest.

Ethics approval and consent to participate

Institutional Review Board approval was obtained. The Ethics approval numbers were Center 1 - 2021124, Center 2 - B2021-214-01, and Center 3 - KYKT2002-069. All patient data accessed complied with relevant data protection and privacy regulations, in accordance with the national legislation and institutional requirements. Written informed consent was waived by the Institutional Review Board.

Consent for publication

Not applicable

REFERENCES

1. Llovet JM, Kelley RK, Villanueva A, et al. Hepatocellular carcinoma. *Nat Rev Dis Primers*. 2021;7:6. Erratum in: Nat Rev Dis Primers 2024;10:10. DOI
2. Mak LY, Cruz-Ramón V, Chinchilla-López P, et al. Global epidemiology, prevention, and management of hepatocellular carcinoma. *Am Soc Clin Oncol Educ Book*. 2018;38:262-79. DOI
3. Shinkawa H, Tanaka S, Kabata D, et al. The prognostic impact of tumor differentiation on recurrence and survival after resection of hepatocellular carcinoma is dependent on tumor size. *Liver Cancer*. 2021;10:461-72. DOI PubMed PMC
4. Saito A, Toyoda H, Kobayashi M, et al. Prediction of early recurrence of hepatocellular carcinoma after resection using digital pathology images assessed by machine learning. *Mod Pathol*. 2021;34:417-25. DOI PubMed PMC
5. Li P, Wu L, Li Z, et al. Spleen radiomics signature: a potential biomarker for prediction of early and late recurrences of hepatocellular carcinoma after resection. *Front Oncol*. 2021;11:716849. DOI PubMed PMC
6. Wang W, Guo Y, Zhong J, et al. The clinical significance of microvascular invasion in the surgical planning and postoperative sequential treatment in hepatocellular carcinoma. *Sci Rep*. 2021;11:2415. DOI PubMed PMC
7. Niu ZS, Niu XJ, Wang WH. Genetic alterations in hepatocellular carcinoma: An update. *World J Gastroenterol*. 2016;22:9069-95. DOI PubMed PMC
8. Su H, Han C, He Y, et al. Molecular mechanism of CK19 involved in the regulation of postoperative recurrence of HBV-associated primary hepatocellular carcinoma in Guangxi. *Ann Transl Med*. 2021;9:1780. DOI PubMed PMC
9. Uenishi T, Kubo S, Yamamoto T, et al. Cytokeratin 19 expression in hepatocellular carcinoma predicts early postoperative recurrence. *Cancer Sci*. 2003;94:851-7. DOI PubMed PMC
10. Zheng Z, Guan R, Jianxi W, et al. Microvascular invasion in hepatocellular carcinoma: a review of its definition, clinical significance, and comprehensive management. *J Oncol*. 2022;2022:9567041. DOI PubMed PMC
11. Pommergaard HC, Rostved AA, Adam R, et al; European Liver and Intestine Transplant Association (ELITA). vascular invasion and survival after liver transplantation for hepatocellular carcinoma: a study from the european liver transplant registry. *HPB (Oxford)*. 2018;20:768-75. DOI
12. Erstad DJ, Tanabe KK. Prognostic and therapeutic implications of microvascular invasion in hepatocellular carcinoma. *Ann Surg Oncol*. 2019;26:1474-93. DOI PubMed
13. Qin SD, Zhang J, Qi YP, Zhong JH, Xiang BD. Individual and joint influence of cytokeratin 19 and microvascular invasion on the prognosis of patients with hepatocellular carcinoma after hepatectomy. *World J Surg Oncol*. 2022;20:209. DOI PubMed PMC
14. Durnez A, Verslype C, Nevens F, et al. The clinicopathological and prognostic relevance of cytokeratin 7 and 19 expression in hepatocellular carcinoma. A possible progenitor cell origin. *Histopathology*. 2006;49:138-51. DOI
15. Govaere O, Komuta M, Berkers J, et al. Keratin 19: a key role player in the invasion of human hepatocellular carcinomas. *Gut*. 2014;63:674-85. DOI PubMed PMC
16. Lee JS, Heo J, Libbrecht L, et al. A novel prognostic subtype of human hepatocellular carcinoma derived from hepatic progenitor cells. *Nat Med*. 2006;12:410-6. DOI
17. Zhuo JY, Lu D, Tan WY, Zheng SS, Shen YQ, Xu X. CK19-positive Hepatocellular carcinoma is a characteristic subtype. *J Cancer*. 2020;11:5069-77. DOI PubMed PMC
18. Kim H, Choi GH, Na DC, et al. Human hepatocellular carcinomas with "Stemness"-related marker expression: keratin 19 expression and a poor prognosis. *Hepatology*. 2011;54:1707-17. DOI
19. Lee K, Lee KB, Jung HY, et al. The correlation between poor prognosis and increased yes-associated protein 1 expression in keratin 19 expressing hepatocellular carcinomas and cholangiocarcinomas. *BMC Cancer*. 2017;17:441. DOI PubMed PMC
20. Yang XR, Xu Y, Shi GM, et al. Cytokeratin 10 and cytokeratin 19: predictive markers for poor prognosis in hepatocellular carcinoma patients after curative resection. *Clin Cancer Res*. 2008;14:3850-9. DOI
21. Choi JY, Lee JM, Sirlin CB. CT and MR imaging diagnosis and staging of hepatocellular carcinoma: part I. Development, growth, and spread: key pathologic and imaging aspects. *Radiology*. 2014;272:635-54. DOI PubMed PMC
22. Murakami T, Sofue K, Hori M. Diagnosis of hepatocellular carcinoma using Gd-EOB-DTPA MR imaging. *Magn Reson Med Sci*. 2022;21:168-81. DOI PubMed PMC
23. Huang X, Long L, Wei J, et al. Radiomics for diagnosis of dual-phenotype hepatocellular carcinoma using Gd-EOB-DTPA-enhanced MRI and patient prognosis. *J Cancer Res Clin Oncol*. 2019;145:2995-3003. DOI PubMed PMC
24. Joo I, Lee JM, Lee DH, Jeon JH, Han JK, Choi BI. Noninvasive diagnosis of hepatocellular carcinoma on gadoxetic acid-enhanced MRI: can hypointensity on the hepatobiliary phase be used as an alternative to washout? *Eur Radiol*. 2015;25:2859-68. DOI
25. Chernyak V, Fowler KJ, Kamaya A, et al. Liver imaging reporting and data system (LI-RADS) version 2018: Imaging of

hepatocellular carcinoma in at-risk patients. *Radiology*. 2018;289:816-30. DOI PubMed PMC
26. Qin Q, Deng LP, Chen J, et al. The value of MRI in predicting hepatocellular carcinoma with cytokeratin 19 expression: a systematic review and meta-analysis. *Clin Radiol*. 2023;78:e975-84. DOI
27. Huang M, Liao B, Xu P, et al. Prediction of microvascular invasion in hepatocellular carcinoma: preoperative Gd-EOB-DTPA-dynamic enhanced MRI and histopathological correlation. *Contrast Media Mol Imaging*. 2018;2018:9674565. DOI PubMed PMC
28. Wang W, Gu D, Wei J, et al. A radiomics-based biomarker for cytokeratin 19 status of hepatocellular carcinoma with gadoxetic acid-enhanced MRI. *Eur Radiol*. 2020;30:3004-14. DOI
29. Feng ST, Jia Y, Liao B, et al. Preoperative prediction of microvascular invasion in hepatocellular cancer: a radiomics model using Gd-EOB-DTPA-enhanced MRI. *Eur Radiol*. 2019;29:4648-59. DOI
30. Yip SS, Aerts HJ. Applications and limitations of radiomics. *Phys Med Biol*. 2016;61:R150-66. DOI PubMed PMC
31. Chen Y, Chen J, Zhang Y, et al. Preoperative prediction of cytokeratin 19 expression for hepatocellular carcinoma with deep learning radiomics based on gadoxetic acid-enhanced magnetic resonance imaging. *J Hepatocell Carcinoma*. 2021;8:795-808. DOI PubMed PMC
32. Wang T, Li Z, Yu H, et al. Prediction of microvascular invasion in hepatocellular carcinoma based on preoperative Gd-EOB-DTPA-enhanced MRI: comparison of predictive performance among 2D, 2D-expansion and 3D deep learning models. *Front Oncol*. 2023;13:987781. DOI PubMed PMC
33. Crawshaw M. Multi-task learning with deep neural networks: a survey. ArXiv: 2009.09796, 20206 [Preprint]. 2020 [cited 2025 Apr 23]: [43 p.]. Available from: https://arxiv.org/abs/2009.09796.
34. Zhao Y, Wang X, Che T, Bao G, Li S. Multi-task deep learning for medical image computing and analysis: A review. *Comput Biol Med*. 2023;153:106496. DOI
35. Caruana R. Multitask Learning. *Machine Learning*. 1997;28:41-75. DOI
36. Chu T, Zhao C, Zhang J, et al. Application of a convolutional neural network for multitask learning to simultaneously predict microvascular invasion and vessels that encapsulate tumor clusters in hepatocellular carcinoma. *Ann Surg Oncol*. 2022;29:6774-83. DOI PubMed PMC
37. Fan M, Yuan W, Zhao W, et al. Joint prediction of breast cancer histological grade and Ki-67 expression level based on DCE-MRI and DWI radiomics. *IEEE J Biomed Health Inform*. 2020;24:1632-42. DOI
38. Xu P, Zeng M, Liu K, Shan Y, Xu C, Lin J. Microvascular invasion in small hepatocellular carcinoma: is it predictable with preoperative diffusion-weighted imaging? *J Gastroenterol Hepatol*. 2014;29:330-6. DOI
39. Cong WM, Bu H, Chen J, et al; Guideline committee. practice guidelines for the pathological diagnosis of primary liver cancer: 2015 update. *World J Gastroenterol*. 2016;22:9279-87. DOI PubMed PMC
40. Zhang X, Li J, Shen F, Lau WY. Significance of presence of microvascular invasion in specimens obtained after surgical treatment of hepatocellular carcinoma. *J Gastroenterol Hepatol*. 2018;33:347-54. DOI
41. Lee S, Kim SH, Lee JE, Sinn DH, Park CK. Preoperative gadoxetic acid-enhanced MRI for predicting microvascular invasion in patients with single hepatocellular carcinoma. *J Hepatol*. 2017;67:526-34. DOI
42. Cong WM, Wu MC. New insights into molecular diagnostic pathology of primary liver cancer: Advances and challenges. *Cancer Lett*. 2015;368:14-9. DOI PubMed
43. Kim H, Jang M, Park YN. Histopathological variants of hepatocellular carcinomas: an update according to the 5th edition of the who classification of digestive system tumors. *J Liver Cancer*. 2020;20:17-24. DOI PubMed PMC
44. Zhang H, Wu C, Zhang Z, et al. , ResNeSt: split-attention networks. In: Gupta M, Patel V, Souvenir R, Editors. Proceedings of 2022 IEEE/CVF Conference on Computer Vision and Pattern Recognition Workshops (CVPRW); 2022 Jun 18-24; New Orleans, LA, USA. Piscataway: IEEE. 2022. pp. 2735-45. DOI
45. He K, Zhang X, Ren S, et al. Deep residual learning for image recognition. In: Bajcsy R, Li FF, Tuytelaars T, Agapito L, Berg T, Kosecka J, Zelnik-Manor L, Editors. Proceedings of 2016 IEEE Conference on Computer Vision and Pattern Recognition (CVPR); 2016 Jun 27-30; Las Vegas, NV, USA. Piscataway: IEEE. 2016. pp. 770-8. DOI
46. Tan M, Le QV. Efficientnet: rethinking model scaling for convolutional neural networks. arXiv:1905.11946 [Preprint]. 2019: [cited 2025 Apr 23] [11 p.]. Available from: https://doi.org/10.48550/arXiv.1905.11946.
47. Caruana R, Sa VRD. Promoting poor features to supervisors: some inputs work better as outputs. In: Jordan MI, Kearns MJ, Solla SA, Editors. Proceedings of the 10th International Conference on Neural Information Processing Systems; 1996 Dec 1-6; Denver, CO, USA. Cambridge: MIT Press. 1996. pp. 278-84.
48. Misra I, Shrivastava A, Gupta A, et al. A. G. Cross-stitch networks for multi-task learning. In: Bajcsy R, Li FF, Tuytelaars T, Editors. Proceedings of 2016 IEEE Conference on Computer Vision and Pattern Recognition (CVPR); 2016 Jun 27-30; Las Vegas, NV, USA. Piscataway: IEEE. 2016. 3994-4003. DOI
49. Jaderberg M, Simonyan K, Zisserman A, et al. Spatial transformer networks. arXiv:1506.02025v3 [Preprint]. 2016: [cited 2025 Apr 23] [15 p]. Available from: https://doi.org/10.48550/arXiv.1506.02025.
50. Santoro A, Raposo D, Barrett DGT, et al. A simple neural network module for relational reasoning. arXiv:1706.01427v1 [Preprint]. 2017: [cited 2025 Apr 23] [16 p] Available form: https://doi.org/10.48550/arXiv.1706.01427.
51. Yang F, Wan Y, Xu L, et al. MRI-radiomics prediction for cytokeratin 19-positive hepatocellular carcinoma: a multicenter study. *Front Oncol*. 2021;11:672126. DOI PubMed PMC
52. Hervella ÁS, Rouco J, Novo J, Ortega M. Multi-adaptive optimization for multi-task learning with deep neural networks. *Neural Netw*.

2024;170:254-65. DOI PubMed

53. Zhang Y, Lv X, Qiu J, et al. Deep learning with 3D convolutional neural network for noninvasive prediction of microvascular invasion in hepatocellular carcinoma. *J Magn Reson Imaging.* 2021;54:134-43. DOI

54. Sun BY, Gu PY, Guan RY, et al. Deep-learning-based analysis of preoperative MRI predicts microvascular invasion and outcome in hepatocellular carcinoma. *World J Surg Oncol.* 2022;20:189. DOI PubMed PMC